# A molecular dynamics study on thermal conductivity of thin epoxy polymer sandwiched between alumina fillers in heat-dissipation composite material

Kouichi Tanaka,[a,b,*] Shuji Ogata,[b] Ryo Kobayashi,[b] Tomoyuki Tamura,[b] and Takahisa Kouno[b,c]

[a]*DENSO CORPORATION, 1-1 Showa-cho, Kariya, Aichi 448-8661, Japan*

[b]*Graduate School of Engineering, Nagoya Institute of Technology, Gokiso-cho, Nagoya, Aichi 466-8555, Japan*

[c]*Institute for Solid State Physics, The University of Tokyo,5-1-5 Kashiwanoha, Kashiwa, Chiba 277-8581, Japan*

[*]*Corresponding author: E-mail address: kouichi_a_tanaka@denso.co.jp; Phone number: +81-566-55-6791*

## Abstract

The composite of epoxy polymers and α-alumina fillers is used as a heat dissipation material. The fillers often agglomerate with nanometer-depth polymers sandwiched in between. We address theoretically the effective thermal conductivity of such a filler-polymer-filler system. The non-equilibrium molecular dynamics simulation is performed to obtain the effective thermal conductivity of the system, in which bisphenol-A (bisA) epoxy polymer sub-system with depth $14-70$ Å is inserted between two α-alumina slabs. Effects of surface-coupling (SC) agent are also investigated by adding model molecules to the polymer sub-system. For smaller polymer-depth cases, the effective thermal conductivity is determined essentially by the interfacial thermal conductance that relates to the temperature-gaps at the interfaces. We find for the interfacial thermal conductance that: (i) it is decreased by decreasing the polymer depth toward the chain length of a single bisA molecule, and (ii) it is increased by adding the SC molecules to the polymer sub-system. Combining separate simulation analyses, we show that the (i) results from effectively weakened interaction between a bisA molecule and two α-alumina slabs due to the orientation constraint on the bisA molecule by the slabs. Reasons of the (ii) are enhancement of the following three quantities by addition of the SC molecules: the phonon population of the bisA molecules at those frequencies corresponding to that of acoustic phonons of α-alumina, the phonon transmission coefficient from the α-alumina slab to the polymer sub-system for the transverse acoustic phonon, and the group velocity of the transverse acoustic phonon in the polymer sub-system.

**Keywords**: thermal conductivity, molecular dynamics, epoxy polymer, alumina, heat dissipation material, composite material

## 1. INTRODUCTION

Heat dissipation materials are essential not only for compact electrical devices but also for automobiles because the temperatures of their electronic components must be kept below certain levels [1-3]. For automobiles, a growing trend exists toward high-density packaging of the electronic components and intense use of power IC's due to the spread of various kinds of electric and hybrid vehicles. Improvement of the heat dissipation material is highly desired. The heat-dissipation material needs be soft to cover the power IC without gaps and electrically insulating [4]. The composite of soft polymer resin and hard filler-particles (called fillers) is often used for such a heat-dissipation material. The fillers, which are about 1−10 micrometer in size, are made of a material with a high thermal conductivity as alumina than the polymers [5,6].

Various experimental trials were performed to further increase the thermal conductivity of such a polymer-ceramic composite: increasing the packing fraction of fillers and using a material with a higher thermal conductivity as boron nitride for the fillers [7-10]. However, the enhancement factors of the thermal conductivity of the composite were behind the expectation due to low interfacial thermal conductance between the filler and polymers. A candidate technique to increase the interfacial thermal conductance is coating the fillers by the surface coupling (SC) agent, which is made of organic molecules and acts to connect the fillers and polymers tightly. It was demonstrated experimentally that addition of the silane coupling agent, in fact, increases the effective thermal conductivity significantly at a high packing fraction of the α-alumina fillers [9,10]. Theoretical understanding of its mechanisms is highly desired to clarify the theoretical upper limit and to design a better SC agent for the composite material.

The interface in the polymer-ceramic composite is characterized as the system of soft polymer and hard crystalline sub-systems. The phonons in a sub-system are scattered partly at the interface not only by the differences in stiffness and mass density but also by the randomness and reconstructed structures. Such phonon scattering events create a temperature gap at the interface, which relates to the interfacial thermal conductance [11-13]. Sophisticated analytical theories exist to predict the interfacial thermal conductance of ideal interface of two homogeneous sub-systems [14,15]. However, their application to the polymer-ceramic composite is difficult because the polymer sub-system is essentially an entangled chains and hence neither homogeneous nor isotropic at microscopic scales. The non-equilibrium molecular dynamics (NEMD) simulation with a realistic setting is best suited to address the issue of interfacial thermal conductance in the polymer-ceramic composite [16-19].

As for the situation of small packing fraction of fillers, we investigated the effects of the

SC molecules on the interfacial thermal conductance by considering the interface system of thick polymers and filler [20]. The bisphenol-A (bisA) epoxy molecules were considered for the polymers, α-alumina for the filler, and a model molecule for the SC. The NEMD simulation was performed for the system at various settings. Increasing either number or chain-lengths of the SC molecules increased the interfacial thermal conductance significantly up to a saturation value. The saturation resulted from a void formation between the α-alumina and bisA by addition of the SC molecules.

In the present paper we will consider the situation of a high packing fraction of α-alumina fillers with/without the SC molecules. We will treat a system where a nanometer-depth polymer sub-system is sandwiched between two α-alumina slabs; that is, it contains two interfaces. We will first perform a series of the NEMD runs by changing the polymer depth and adding the SC molecules to understand their effects on the interfacial thermal conductance. We will show that the interfacial thermal conductance is decreased significantly by decreasing the depth of the polymer sub-system without the SC molecules toward the chain-length of a bisA molecule, and that the interfacial thermal conductance is increased by adding the SC molecules. We will explain their microscopic mechanisms through combined analyses of the polymer configurations, atomic vibration spectra of the polymer sub-system [21,22], and phonon wave-packet dynamics simulation [23-26].

The remaining sections are organized as follows. In Sec. 2, atomistic modeling of the simulation system with the inter-atomic potentials will be explained. Section 3 will perform the NEMD simulation at various settings of the polymer depth with/without the SC molecules to understand their effects on the interfacial thermal conductance. Section 4 will perform the atomic vibration spectra analysis through the equilibrium MD simulation to clarify the changes in the vibrational properties of the polymer sub-system by decreasing its depth and by adding the SC molecules. It will explain reasons for the changes in the interfacial thermal conductance obtained in Sec. 3. Section 5 will perform the phonon wave-packet dynamics simulation to evaluate further the mode-dependent transmission coefficient through the interface and the group velocity in the polymer sub-system. Discussion and concluding remarks will be given in Sec. 6.

## 2. MODELING OF SYSTEM AND INTER-ATOMIC POTENTIALS

We assume α-alumina for the filler and bisphenol-A epoxy (bisA) molecules for the polymers because both are commonly used for the electrically insulating heat-dissipation composite material [2,27,28]. We consider (0001) surface of α-alumina with Al termination as the filler surface, which is the most stable one [29-31]. Figure 1 (a) shows the present model of the bisA molecule, in which two epoxy groups terminate the two ends. It is known experimentally that

various degrees of polymerization through bonding reaction of the epoxy groups occur for the bisA molecules [32]. However, we here take the simplest model (Fig. 1 (a)) from the following reasons: (i) Irrespective of the degree of polymerization, two epoxy groups remain at the two ends. (ii) Essential physics are expected to depend on the ratio of the chain length of a bisA molecule to the depth of the polymer sub-system. (iii) Recent papers have used the present simple model as a fundamental one for the cross-link reactions [33,34].

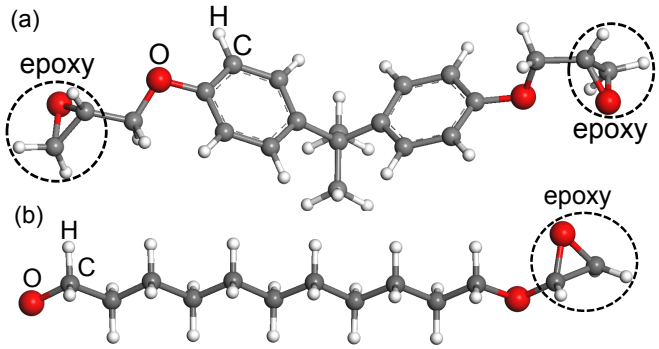


FIG.1

FIG. 1. (Color online) (a) Structure of bisphenol-A (bisA) epoxy model molecule. (b) Structure of surface coupling (SC) model molecule.

For the surface-coupling agent, the silane composite molecules [10] are often used in experiments. The silane composite molecule is basically composed of two kinds of groups attached to a Si atom: the reaction group (e.g., epoxy) bonds to a bisA molecule, the OR group (e.g., -O-$CH_3$) undergoes the hydrolysis reaction to form a bond between the O and a surface Al of α-alumina filler. The silane composite molecule thereby works to bind α-alumina and bisA molecule together. In the present simulation we use a virtual surface-coupling (SC) molecule shown in Fig. 1 (b) that mimics the molecular state after the hydrolysis reaction: an epoxy group connects to $(CH_2)_n$ while the other end of $(CH_2)_n$ is saturated with an O atom. We set $n = 11$. The chain-lengths of bisA and SC molecules are both about 20 Å.

We use the two-body inter-atomic interaction potentials for Al and O in α-alumina in the CMAS potential suite [35]. The suite has been widely used for the MD simulation of CaO, MgO, α-alumina, and $SiO_2$ systems. The Dreiding inter-atomic potentials [36] are adopted for the bisA and SC molecules. Following the Gasteiger-Marsili method [37], we obtain the atomic charges for the bisA and SC molecules. We need to construct the inter-atomic potential between α-alumina and SC molecule, which is essential in the present MD simulation. Since the O atom at the end of the SC molecule bonds tightly to a surface Al atom in the electronic density-functional theory (DFT) with PBE-GGA, we use the Al-O potential calculated by the DFT and fitted to the Morse form as explained in Ref. 20. For the remaining inter-atomic potentials between α-alumina and SC molecules as well as the inter-atomic potentials between α-alumina and bisA molecules, we adopt the dispersion and Coulomb terms in the CMAS and Dreiding with the Lorentz-Berthelot mixing

rule (i.e., arithmetic and geometric means for the diameter and energy factors, respectively).

## 3. NON-EQUILIBRIUM MOLECULAR DYNAMICS (NEMD) SIMULATION

We consider the alumina-polymer-alumina system corresponding to the situation of high packing fraction of fillers in the composite for the NEMD simulation. Since the thermal conductivity of α-alumina is orders of magnitude higher than that of bulk bisA, we can reduce the size of α-alumina for fast NEMD simulation. Figure 2 (top) depicts a typical configuration of the system for the NEMD simulation. The two α-alumina slabs with Al termination are placed on the left and right sides of the simulation box, while the polymer sub-system of depth $D$ with or without the SC molecules are placed in between. The $z$-axis is set perpendicular to the interface as shown in Fig. 2. The periodic boundary conditions are applied for the $x$, $y$, and $z$-directions. To reduce long-range Coulomb interaction with the image slabs, two vacuum layers of $20$ Å depth are set at both ends of the simulation box, and the dipole correction [38] is applied to the Ewald method. The left (right) end of the left (right) α-alumina slab is fixed during a simulation run. The high and low temperature-controlled regions, at $T = 430$ and 370 K, are set in the α-alumina slabs to input and subtract the kinetic energies.

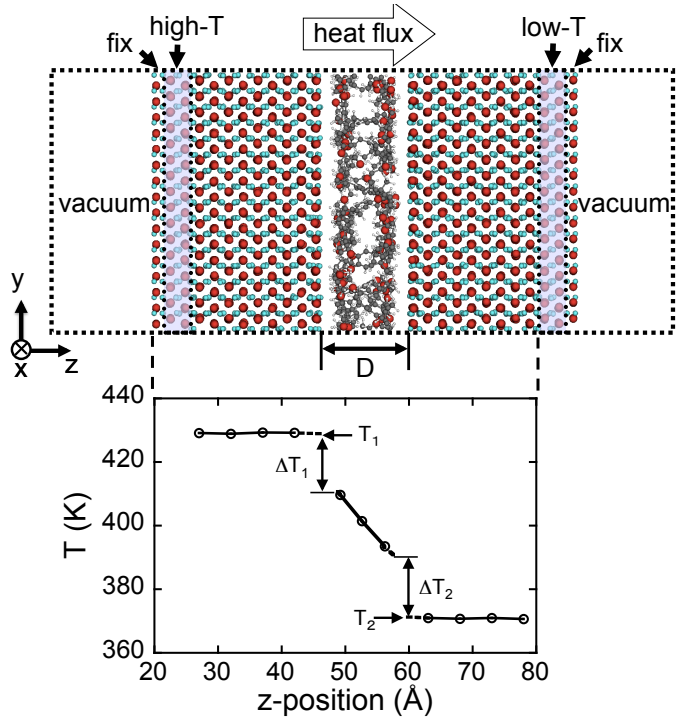


FIG.2

FIG. 2. (Color online) (top) Atomic configuration of a typical system for the NEMD simulation with $D = 14$ Å without the SC molecules. Large red spheres are O's; medium cyan, Al's; medium grey, C's; small white, H's. (bottom) The temperature profile obtained in the NEMD run. Each point corresponds to the averaged kinetic energy of C, O, and Al-atoms in each 5.0 Å $z$-widths.

Various values of the polymer depth, $D$, are considered. When the polymer sub-system contains no SC molecules, $L_z = 106,\ 125$, and $153$ Å for $D = 14,\ 33$, and $61$ Å, respectively. The $L_x$ and $L_y$ are fixed respectively to $34$ Å and $38$ Å, which are sufficiently longer that the chain length of a bisA molecule (~20 Å). The bisA molecules form an amorphous solid with nearly the same mass density of $0.86 - 0.88\ \mathrm{g/cm^3}$ in all cases. In the case of $D = 14$ Å, the system is composed of 8,660 atoms. We also consider the cases with the SC molecules inserted in the polymer sub-system. Total of 16 SC molecules are placed on the interface in a square lattice form $(4\times2)$ with their end atoms (O) bonded to surface Al's of two α-alumina surfaces. At the addition of the SC molecules we increase $L_z$ from the original value to keep the mass density of the polymer sub-system to $0.86 - 0.89\ \mathrm{g/cm^3}$.

The velocity-Verlet algorithm is used to integrate the equations of atomic motion [39]. We set the time step $dt = 1.0$ fs from detailed analyses [20] about the $dt$-dependencies of the temperature profile and energy flux in preparation runs. We omit H atoms in calculating the temperature profile. We confirm that the system is in the steady state after 1.5 ns by checking the difference between the input and subtracted energies per unit time in the temperature-controlled regions. The energy (heat) flux and temperature profile are obtained by averaging over 0.5 ns in the steady state.

Figure 2 (bottom) depicts the temperature profile for the case of $D = 14$ Å without the SC molecules. The temperature gradient is quite small in the α-alumina, while substantial in the bisA. The temperature-gaps $\Delta T_1$ and $\Delta T_2$ at the interfaces are significant. Majority of the thermal resistance of the polymer sub-system originates from such temperature gaps. The temperatures at the end $z$-positions of the α-alumina and bisA in close proximity to the interfaces are determined as follows. First, the end $z$-positions are defined as $z = 46$ Å for the α-alumina and $z = 48$ Å for the bisA for the left interface; $z = 58$ Å for the bisA and $z = 60$ Å for the α-alumina for the right interface. Since the end $z$-position of the bisA fluctuates in time and varies depending on the $x$-$y$ location, we define it as the one separated by $2$ Å from the $z$-end (i.e., Al) of α-alumina. Then, the temperatures at those end $z$-positions are determined through linear extrapolation of data points (the open circles in Fig. 2 (bottom)).

We define the effective thermal conductivity of the polymer sub-system by

$$\Lambda = JD/(T_1 - T_2), \qquad (1)$$

where $J$ is the heat flux per surface area and $T_1$ and $T_2$ are the high and low temperatures at the end $z$-positions of the α-alumina's at the interfaces. The effective thermal conductivity between two α-alumina's is a useful quantity to predict the effective thermal conductance of the whole composite

material. Figure 3 shows the *D*-dependence of $\Lambda$. We find in Fig. 3 that for both cases with and without the SC molecules, $\Lambda$ decreases linearly as *D* decreases. Without the SC molecules, $\Lambda$ for $D = 14$ Å is about 50 % of that for $D = 61$ Å. With the SC molecules, $\Lambda$ decreases by 20 % only when we change *D* from 67 Å to 19 Å.

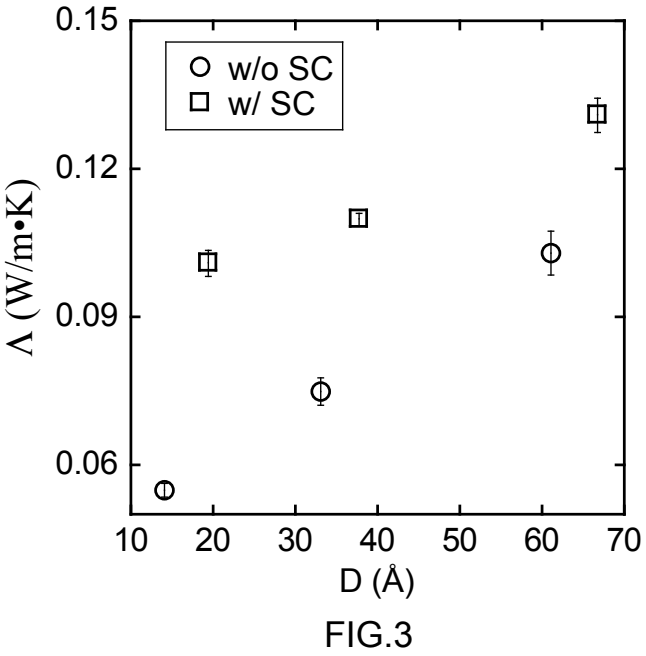

FIG.3

FIG. 3. The effective thermal conductivities (Eq. 1) of the polymer sub-systems for various values of $D$ with or without the SC molecules.

The $\Lambda$ of the polymer sub-system is composed of the thermal conductivity of the polymers and the interfacial thermal conductance. The thermal conductivity of the polymers is defined as

$$\lambda = J/\left(\frac{dT}{dz}\right), \quad (2)$$

where the temperature gradient $dT/dz$ is obtained at the central region of the polymers. The interfacial thermal conductance is defined as

$$J/\Delta T \text{ with } \Delta T = (\Delta T_1 + \Delta T_2)/2, \quad (3)$$

where $\Delta T_1$ and $\Delta T_2$ are the temperature-gaps depicted in Fig. 2 (bottom). We note that the differences between $\Delta T_1$ and $\Delta T_2$ are smaller that 3 K in the present runs. Though the interfacial thermal conductance depends generally on the direction of heat flow [40,41], we cannot see substantial dependences. Figure 4 shows $\lambda$ and $J/\Delta T$ for the cases without the SC molecules. In the case of $D = 14$ Å without the SC molecules, $\lambda = 0.10\ \mathrm{W/m \cdot K}$ is close to that of the bulk bisA ($0.11 - 0.13\ \mathrm{W/m^2 \cdot K}$) [20]. On the other hand, $J/\Delta T$ for the case of $D = 14$ Å without the SC molecules is only about 50 % of that for the cases of $D = 33$ and 61 Å without the SC molecules. We state that the significant linear-decrease in $\Lambda$ for smaller $D$ in Fig. 3 has resulted mainly from such a behavior in $J/\Delta T$.

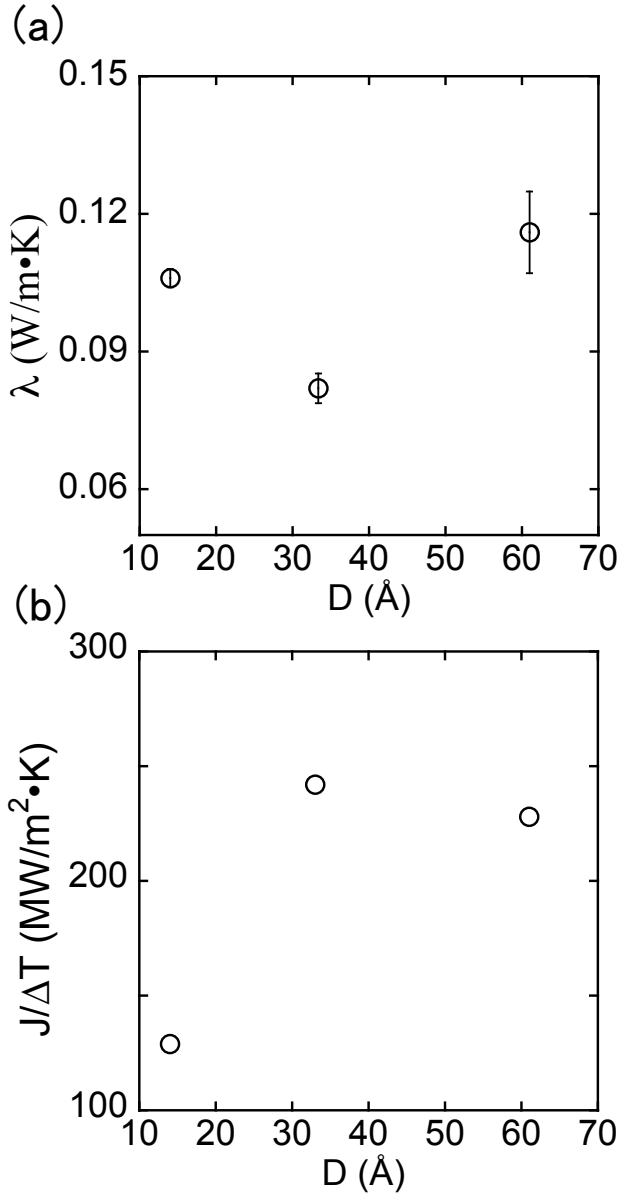


FIG. 4. (a) The thermal conductivities (Eq. 2) of the polymer sub-systems for various values of $D$ without the SC molecules. (b) The interfacial thermal conductances (Eq. 3) for the same cases as (a).

FIG.4

We consider physical reasons of the relatively low interfacial thermal conductance, $J/\Delta T$, between the α-alumina and bisA in the case of $D = 14$ Å without the SC molecules. Figure 5 compares the numbers of the bisA atoms (C and O) in the 1.0 Å $z$-width bins prepared virtually from the α-alumina (left block) surface in the cases of $D = 14$ and $61$ Å without the SC molecules. In both cases, we observe accumulation of the bisA atoms near the α-alumina surface. It is a result of relatively strong Coulomb attraction between the surface Al of the α-alumina and O of the epoxy group in addition to between the O of the α-alumina and H of the bisA. It is noteworthy that the number of the bisA atoms within a few Å from the α-alumina surface is smaller in the $D = 14$ Å case than in the $D = 61$ Å case. It results from the structural stability of a bisA molecule. We find

that the intra-molecular O-O distances between the two epoxy groups are $12.2-14.6$ Å in the $D=14$ Å case and $12.1-14.9$ Å in the $D=61$ Å case. Correspondingly the bending angles in overall V-shape of the bisA molecules are kept in the range of $110-124$ degrees. When $D$ becomes close to the chain length ($\sim$20 Å) of a bisA molecule, substantial fraction of the bisA molecules are oriented to bridge between the two α-alumina slabs through attractive interaction of the O in the epoxy group and Al of α-alumina. In fact, we find that 11 out of 20 bisA molecules are in the bridging state. Such orientation constraint on the bisA molecules in the $D=14$ Å case acts to lower the density of the bisA atoms at the interface as compared to the $D=61$ Å case in which no such a constraint exists. The interfacial thermal conductance, $J/\Delta T$, gets smaller due to the weaker interaction at the interface resulting from lower density of the bisA atoms at the interface.

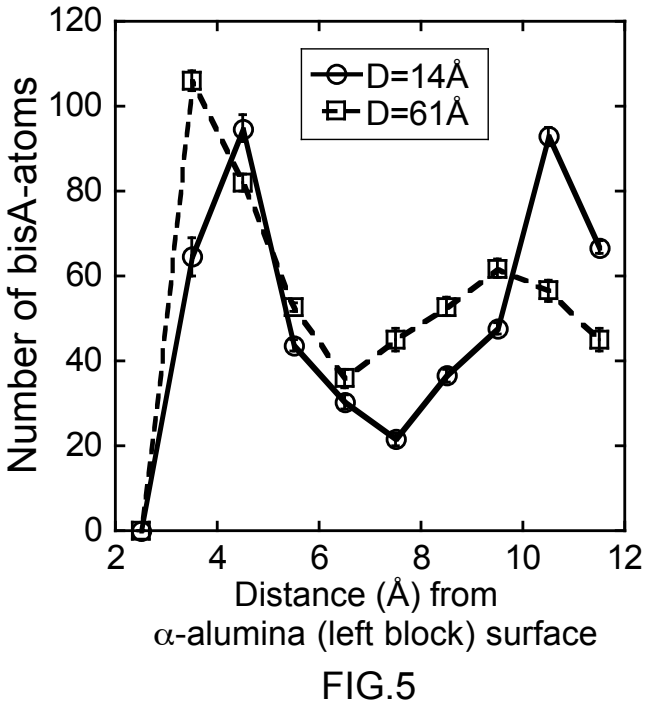


FIG. 5. The numbers of C and O atoms of the bisA molecules in $z$-bins obtained through the NEMD simulation for the systems with $D=14$ Å and 61 Å.

When the SC molecules are added to the system with $D=14$ Å, the effective thermal conductivity of the polymer sub-system, $\Lambda$, becomes 1.8 times as large as the original value. Addition of the SC molecules reduces deterioration of $\Lambda$ of the polymer sub-system for smaller $D$. As depicted in Fig. 6, the SC molecules act to connect the polymers and α-alumina. Hence the interfacial thermal conductance, $J/\Delta T$, increases by about 20 %. Interestingly the thermal conductivity of the polymers, $\lambda$, also becomes 2.0 times as large as that for the case without the SC molecules. Such effects of the SC molecules on the neighboring bisA molecules will be investigated in Sec. 4 through atomic vibration spectra analyses.

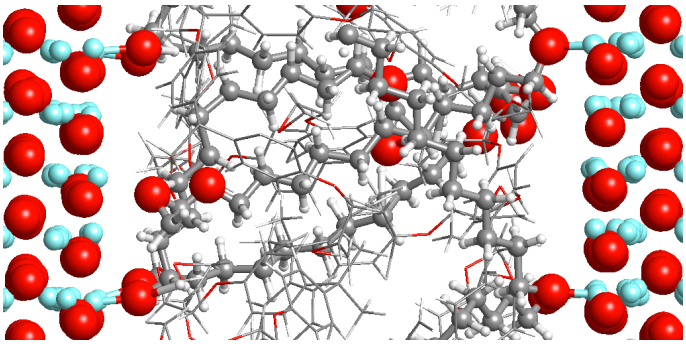

FIG. 6. (Color online) The close-up view of the simulation system for the case of $D = 14$ Å with the SC molecules. The SC molecules are drawn by spheres in the central region. The bisA molecules are drawn by sticks.

FIG.6

## 4. ATOMIC VIBRATATION SPECTRA ANALYSES

The heat flux $J$ per unit area across the interface (normal to $z$-direction) from medium-$a$ at temperature $T = T_a$ to medium-$b$ at $T = T_b$ is expressed in terms of transmitted phonons as

$$J = \frac{1}{V_a}\sum^{+}_{\mathrm{mode},\vec{\eta}} v_{a,z}(\mathrm{mode},\vec{\eta})hf_a(\mathrm{mode},\vec{\eta})P_a(T_a,\mathrm{mode},\vec{\eta})t_{ab}(\mathrm{mode},\vec{\eta})$$
$$+\frac{1}{V_b}\sum^{-}_{\mathrm{mode},\vec{\eta}} v_{b,z}(\mathrm{mode},\vec{\eta})hf_b(\mathrm{mode},\vec{\eta})P_b(T_\mathrm{b},\mathrm{mode},\vec{\eta})t_{ba}(\mathrm{mode},\vec{\eta}) \qquad (4)$$

with the volumes $V$'s, phonon group velocities $v$'s, phonon frequencies $f$'s, phonon populations $P$'s, and transmission coefficients $t$'s. The summations are performed over the acoustic phonons, characterized with the wavelength vector $\vec{\eta}$ and transverse or longitudinal mode, in the first Brillouin zone with the direction of crossing the interface. It is assumed that the incident phonon keeps its frequency after crossing the interface. To clarify the situation, we here assume that medium-$a$ is a hard crystalline material, e.g., α-alumina and that medium-$b$ is a soft one, e.g, polymers. In the limit of $T_a = T_b$, the partial flux from medium-$a$ to $b$ should cancel with the one from medium-$b$ to $a$, from the principles of detailed balance. To have a higher interfacial thermal conductance, such partial fluxes need be larger.

As for the first term on the right hand side of Eq. (4) (i.e., the partial flux from medium-$a$ to $b$), only $t_{ab}$ can change by decreasing $D$ or addition of the SC molecules due to the hardness of medium-$a$. On the other hand, all the terms in the second term on the right hand side of Eq. (4) (i.e., the partial flux from medium-$b$ to $a$) can change. In this section we will suggest that addition of the SC molecules to the polymer sub-system in the present model enhances the phonon population ($P_b$) of medium-$b$ in the acoustic frequency range of medium-$a$. Corresponding enhancement in $t_{ab}$ as well as in $v_{b,z}$ will be studied in Sec. 5 through the wave-packet dynamics simulation.

We begin with evaluating the phonon population of bulk α-alumina at $T = 300$ K. The phonon population at frequency $f$ for a given wavelength vector $\vec{\eta}$ is evaluated through the

equilibrium MD simulation as

$$P_{\mathrm{l}}(f,\vec{\eta}) = \left|\frac{1}{Nn_s}\sum_{j=1}^{N}\sum_{n=0}^{n_s-1}\vec{v}_j(n\Delta t)\cdot\hat{\eta}\exp\left(i\frac{2\pi}{\eta}\vec{r}_j\cdot\hat{\eta}-i2\pi fn\Delta t\right)\right|^2, \quad (5)$$

$$P_{\mathrm{t}}(f,\vec{\eta}) = \left|\frac{1}{Nn_s}\sum_{j=1}^{N}\sum_{n=0}^{n_s-1}\left[\vec{v}_j(n\Delta t)-(\vec{v}_j(n\Delta t)\cdot\hat{\eta})\hat{\eta}\right]\exp\left(i\frac{2\pi}{\eta}\vec{r}_j\cdot\hat{\eta}-i2\pi fn\Delta t\right)\right|^2 \quad (6)$$

for longitudinal and transverse modes, respectively. The $f = f_m \equiv m/n_s\Delta t$ with natural number $m$, $\vec{\eta} = (L_x/n_x, L_y/n_y, L_z/n_z)$ with integer vector $(n_x, n_y, n_z)$, $\hat{\eta} = \vec{\eta}/|\vec{\eta}|$, total number of atoms $N$, number of sampling points $n_s$, and time interval of sampling $\Delta t$. To cover the frequency range $0-10$ THz of our interest, we set $n_s = 6{,}000$ and $\Delta t = 15$ fs. Because of limitation in the total sampling period $t_{\mathrm{total}} \sim 90$ ps, $f$ in Eqs. (5) and (6) may contain uncertainties of $\pi/t_{\mathrm{total}} \sim 0.03$ THz. Therefore $P_{\mathrm{l}}$ ($P_{\mathrm{t}}$) at a given $f_m$ is obtained after averaging over $\pm 5$ data points of $m$ to reduce fluctuation. The system size of α-alumina is $(L_x, L_y, L_z) = (34.0\text{ Å}, 38.0\text{ Å}, 39.0\text{ Å})$ with the periodic boundary conditions. We set the wavelength vector parallel to $z$-direction. We consider the cases of $\eta = 39.0,\ 19.5,$ and $13.0$ Å by setting $n_z = 1, 2,$ and $3$, respectively, which correspond respectively to the wavenumbers $0.33(2\pi/a)$, $0.66(2\pi/a)$, and $2\pi/a$ with the lattice constant $a = 13.0$ Å of α-alumina in (0001)-direction. We set the time step $dt = 1.0$ fs in the MD simulation.

Figure 7 (a) shows the frequency dependencies of $P_{\mathrm{l}}$ and $P_{\mathrm{t}}$ for bulk α-alumina at $T = 300$ K at the three $\vec{\eta}$'s. At the longest wavelength of $\eta = 39.0$ Å, $P_{\mathrm{l}}$ ($P_{\mathrm{t}}$) has a strong and sharp peak at $f = 1.2$ (2.7) THz. At shorter wavelengths, such $P$-peaks spread in frequency, which means shorter life times. Figure 7 (b) shows relative intensities of the $P$-peaks, which appear to follow the Maxwell-Boltzmann statistics of the phonon energy as expected. To plot Fig. 7 (b), intensity of a $P$-peak is calculated by integrating the population around the central frequency (see Fig 7 (a)). The phonon dispersion relation evaluated from Fig. 7 (b) compares well with the one calculated with the DFT calculation. The longitudinal phonon frequency ranges in $0-10$ THz, while the transverse one in $0-5$ THz.

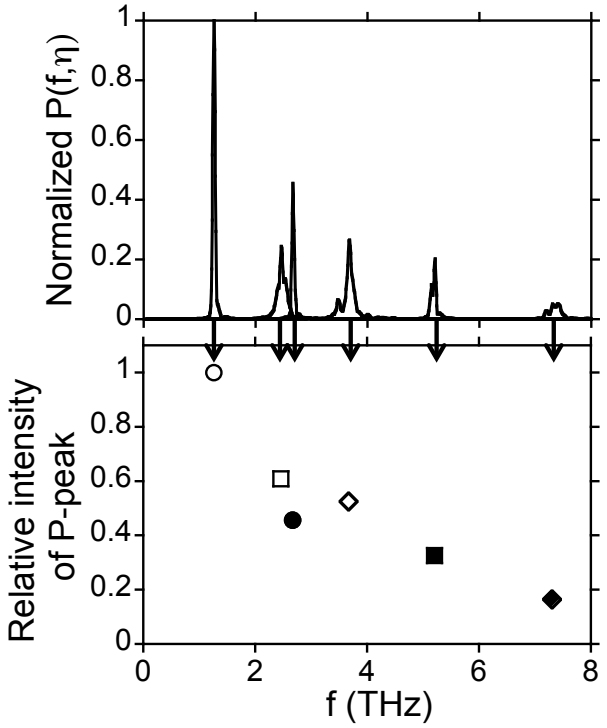


FIG.7

FiG. 7. (a) The $P_{\mathrm{l}}$ and $P_{\mathrm{t}}$ (Eqs. 5 and 6) of bulk α-alumina at $T = 300$ K for three $\vec{\eta}$'s parallel to $z$-direction, normalized by the largest value at $f = 1.2$ THz. (b) Relative intensities of the peaks in (a). The open symbols are for $P_{\mathrm{t}}$; closed ones, for $P_{\mathrm{l}}$.

We now consider the phonon population for the bisA. First we set a single bisA molecule only in a simulation box of $(L_x, L_y, L_z) = (34.0\ \text{Å}, 38.0\ \text{Å}, 39.0\ \text{Å})$ with a connecting vector between the two epoxy O's parallel to $z$-direction; orientation of the vector is kept during the MD run. The average $(2P_{\mathrm{t}} + P_{\mathrm{l}})/3$ for $\eta = 13.0$ Å $(n_z = 3)$ for the case of a single bisA molecule at $T = 100$ K is depicted in the inset of Fig. 8; H atoms are omitted in $P_{\mathrm{l}}$ and $P_{\mathrm{t}}$. In the range of $0 - 8$ THz, as expected, we observe several sharp peaks corresponding to the molecular vibration modes. In the lowest mode of $f = 0.8$ THz, the molecule vibrates as the two epoxy groups flap like a butterfly wings. If the temperature is increases to $T = 300$ K, those peaks decompose to many peaks with substantial broadening. It is a reflection of increased degrees of non-linearity in the inter-atomic potential at a higher temperature. Second we prepare bulk bisA with the same simulation box size. Figure 8 shows the average $(2P_{\mathrm{t}} + P_{\mathrm{l}})/3$ for $\eta = 13.0$ Å $(n_z = 3)$ for the bulk bisA at $T = 300$ K obtained through three MD runs for 120 ps. Significant broadening in Fig. 8 in comparison to Fig. 8 (inset) means that the phonon picture in the wavenumber space may be inappropriate in the case because of the non-linearity in the inter-atomic potential and the randomness in the molecular configurations.

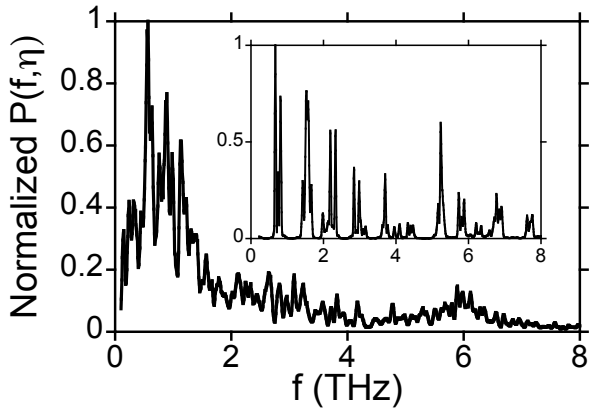


FIG.8

FIG. 8. The average $(2P_{\mathrm{t}} + P_{\mathrm{l}})/3$ of bulk bisA at $T = 300$ K for $\vec{\eta} = (0,0,13.0\text{Å})$. The inset corresponds to the case of a single bisA molecule at $T = 100$ K for the same $\vec{\eta}$.

We therefore integrate over the wavenumbers (inverse of $\vec{\eta}$) in Eqs. (5) and (6) before summation over the atoms for better statistics in analyzing possible changes in the phonon or vibrational-mode population by addition of the SC molecules, which reduces to the vibration spectrum of each atom. It is useful for the purpose to group atoms following the grouping rule used in the Dreiding inter-atomic potential. We therefore calculate

$$P_{\mathrm{group}}(f) = \frac{1}{N_{\mathrm{g}}} \sum_{j=1}^{N_{\mathrm{g}}} \left| \frac{1}{n_s} \sum_{n=0}^{n_s-1} \overrightarrow{v_j}(n\Delta t) \exp(i2\pi f n\Delta t) \right|^2 \qquad (7)$$

for a given group. The groups for the bisA are the following: O atoms are grouped into O1 (epoxy) and O2 (others), C into C2 (benzene) and C1 (others) as depicted in Fig. 9 (a). As for the SC, O into O3 (bonded to Al), O5 (epoxy) and O4 (other), and C into C3. The $N_{\mathrm{g}}$ in Eq. (7) is the number of atoms in a group. We consider $f = 0.30$, 3.0 and 6.0 THz. We note that $f = 0.3$ THz corresponds to the peak in Fig. 8 relating to vibrations of winds (i.e., epoxy groups) of bisA molecules; $f = 3.0$ and 6.0 THz, to typical phonons of α-alumina.

Figure 9 (b) shows $P_{\mathrm{group}}$'s for the bulk bisA at $T = 300$ K, normalized by the value for O1-group at $f = 3.0$ THz. The $P_{\mathrm{group}}$ for O1-group assumes the largest value at $f = 3.0$ THz. This relatively fast vibration at $f$ =3.0 THz is caused by the Coulomb interaction between O1 (charge, $-0.371\,e^-$) and C1 ($0.105\,e^-$) of surrounding molecules. If we make $N_{\mathrm{g}}$-weighted average of $P_{\mathrm{group}}$, that is, simple sum of the absolute squares in Eq. (7) over all the atoms, we find that the population at $f = 0.30$ THz is the largest. Figure 9 (c) shows $P_{\mathrm{group}}$'s in the polymer sub-system for the case of $D = 14$ Å without the SC molecules at equilibrium $T = 300$ K, normalized by the same value used in Fig. 9 (b). As seen in Fig. 9 (c), $P_{\mathrm{group}}$'s at $f = 0.30$ THz are substantially smaller than that for the bulk bisA. As stated in the last section, a bisA molecule in the case of $D = 14$ Å without the SC molecules is effectively constrained by the two α-alumina's.

Those constrained bisA molecules cannot oscillate freely at $f = 0.30$ THz in the butterfly-like mode. We note that such a change at $f = 0.3$ THz does not affect substantially the interfacial thermal conductance because the phonon population at such a low frequency is small for α-alumina. The $P_{\text{group}}$ for O1-group at $f = 3.0$ THz in Fig. 9 (c) is significantly larger that that of the bulk bisA in Fig. 9 (b), while that of the other group (O2) changes little. The change comes from those O1 atoms interacting much with the surface Al's of α-alumina. Though $f = 3.0$ THz corresponds to middle of the acoustic phonon frequency range of α-alumina, the change in $P_{\text{group}}$ for O1-group only has little effect on the thermal conductivity of the polymers, as demonstrated in the last section through the NEMD results. The decrease in the interfacial thermal conductance for the case of $D = 14$ Å without the SC molecules should have resulted from decreased transmission coefficients ($t_{ab}$ and $t_{ba}$) due to decreased local atomic density of the polymers at the interface (see Fig. 5).

The $P_{\text{group}}$'s for the case of $D = 14$ Å with the SC molecules are shown for the bisA molecules in Fig. 9 (e) and for the SC in Fig. 9 (d); both are normalized by the same value used for Fig. 9 (b). As seen in Fig. 9 (e), $P_{\text{group}}$'s for the O1, C1, and C2-groups of the bisA increase significantly at $f = 3.0$ THz by the influence of the SC molecules (see Fig. 9 (d)). We guess that addition of the SC molecules enhances the phonon population of the bisA in the acoustic phonon frequency range of α-alumina by making the bisA effectively stiffer through entanglement of the bisA and SC molecules.

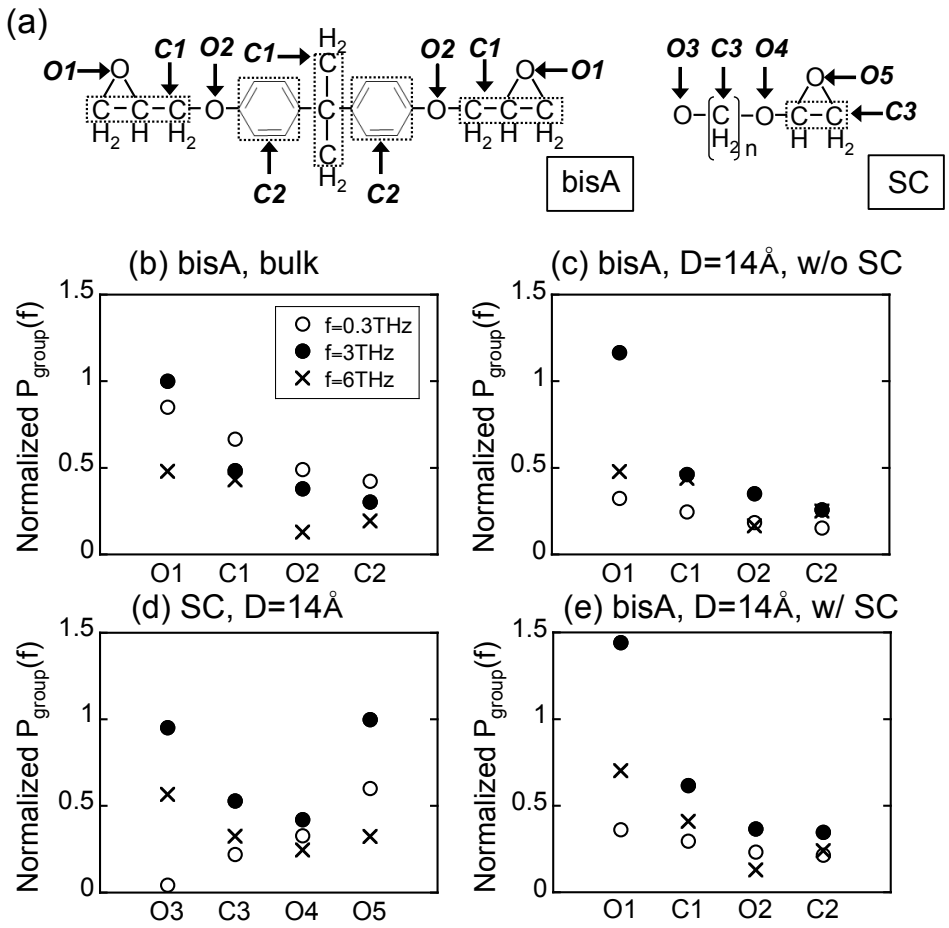


FIG.9

FIG. 9. (a) The grouping of C and O atoms. (b) The $P_{\mathrm{group}}$ of bulk bisA at $T = 300$ K. (c) The $P_{\mathrm{group}}$ of the bisA for the case of $D = 14$ Å without the SC at $T = 300$ K. (d) The $P_{\mathrm{group}}$ of the SC for the case of $D = 14$ Å with the SC at $T = 300$ K. (e) The $P_{\mathrm{group}}$ of the bisA for the case of $D = 14$ Å with the SC at $T = 300$ K.

## 5. PHONON WAVE-PACKET DYNAMICS

As explained in the last section, the interfacial thermal conductance is related to the phonon transmission coefficient and group velocity. The NEMD simulation cannot give such detailed information of the heat transfer. In this section we investigate those issues through the phonon wave-packet dynamics simulation.

In the simulation, we initially set an acoustic phonon wave-packet and then perform an MD run to trace the time evolution of the wave packet. We thereby obtain the transmission

coefficient through the interface for the wave packet characterized by the wavelength and mode (transverse or longitudinal). Figure 10 depicts a typical configuration of the system in the present phonon wave-packet dynamics simulation. We replace the left α-alumina slab used in the NEMD simulation by a thick slab of depth $130$ Å to set a wave packet. We consider the *D*-dependence of the wave-packet transmission. The system sizes are $(L_x, L_y, L_z) = (34\text{Å}, 38\text{Å}, 210\text{Å})$ and $(34\text{Å}, 38\text{Å}, 229\text{Å})$ for the cases of $D = 14$ and 33 Å without the SC molecules, respectively. In addition, we consider the cases with 16 SC molecules to analyze their effects on the transmission; as in the NEMD simulation, $L_z$ is increased from the original value to keep the mass density of the polymer sub-system to $0.86 - 0.89\ \text{g/cm}^3$. To suppress artificial reflection of the wave packet at the ends of the α-alumina slabs, we set damper regions; the damper width is 26.5 Å (5.3 Å) for the left (right) α-alumina slab, as shown in Fig. 10 (top).

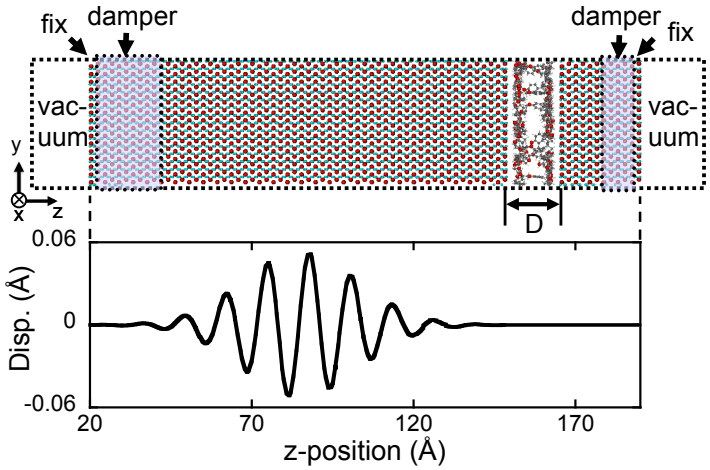


FIG.10

FIG. 10. (Color online) (top) Atomic configuration of the system in the case of $D = 14$ Å without the SC molecules for the wave-packet dynamics simulation. (bottom) The displacement profile applied to the system in (top).

Among acoustic and optical phonons in α-alumina, we consider that the heat transfers mostly through the acoustic phonons due to their large group velocities. To set initially the acoustic wave-packet in the left α-alumina slab, we obtain the minimum energy configuration of atoms under the condition that the averaged displacement $R_{iz}$ of those atoms contained in *i*-th *z*-width of 2.17 Å, which corresponds to one sixth of *c*-axis length (13.0 Å) of the α-alumina unit-cell, is

$$A \sin\frac{2\pi R_{iz}}{\eta} \exp\left(-\frac{(R_{iz}-R_0)^2}{2\sigma^2}\right) \tag{8}$$

with $A = 0.053$ Å, $\sigma = 18$ Å, and the central *z*-position $R_0$ of the wave packet. For high numerical accuracy, we apply small constant forces, which are the reverse of the residual atomic force vectors at the initial configuration, to the atoms in the polymer sub-system. The displacements are parallel to *z*-direction for the longitudinal mode, while *y*-direction for the transverse mode. We consider three wavelengths $\eta = 13.0$, 26.0, and 39.0 Å. By performing the MD simulation we

monitor the time evolutions of the spatial distributions of the kinetic and potential energies. Both are found to show the same behavior. Since the wave-packet dissipates significantly in the polymer sub-system, we focus on analyzing the wave-packet transmission from the α-alumina slab to the polymer sub-system.

Figure 11 shows the transmission coefficients for various combination cases of the wavelength $\eta$, mode (longitudinal or transverse), and with or without SC molecules. Here the transmission coefficient is defined as the ratio in total (i.e., kinetic plus potential) energy increment between the transmitted wave-packet in the polymer sub-system to the incident one in the α-alumina slab. In general the transmission coefficient is larger for larger $\eta$ because it has a smaller frequency and hence can transform to a phonon with the same frequency that exists in the soft polymer. In the following we therefore concentrate on comparing the cases with $\eta = 39.0$ Å to analyze three kinds of effects (*D*, mode, and SC molecules) on the transmission coefficient.

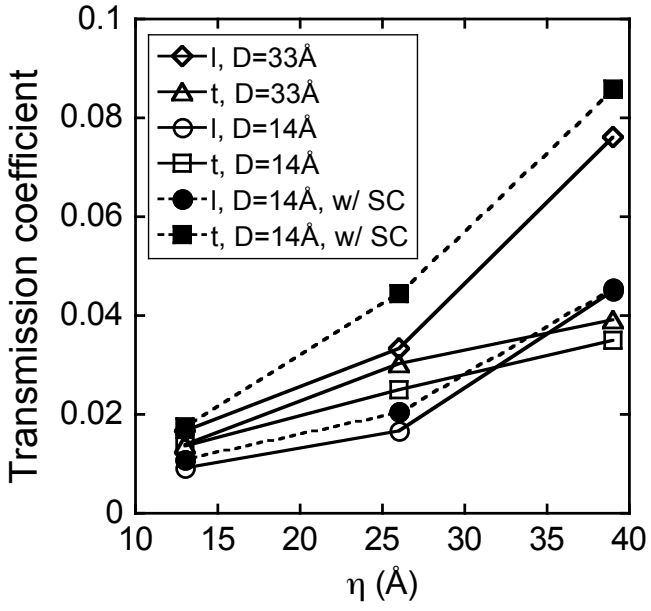


FIG.11

FIG. 11. The transmission coefficients of longitudinal ( l ) and transverse (t ) wave-packets obtained through the wave-packet dynamics simulation for $D = 14$ and 33 Å with or without the SC molecules.

First we analyze the effects of the polymer sub-system depth, *D,* on the transmission coefficient. Since the longitudinal wave involves change in local pressure, surface of the polymer sub-system is forced to move. Accurate determination of the transmission coefficient therefore requires waiting about 1 ps until the possible wave reflection occurs. We thereby find for the longitudinal mode with $\eta = 39.0$ Å that the transmission coefficient is 0.045 for the case of $D = 14$ Å without the SC molecules, while 0.076 for case of $D = 33$ Å without the SC molecules. The significant decrease in the transmission coefficient of longitudinal mode for smaller *D* is related to

the decrease in the interfacial thermal conductance found for smaller $D$ in the NEMD simulation. For the transverse mode, on the other hand, the transmission coefficient changes little.

Second we analyze further the effects of mode on the transmission coefficient. Significant difference in the transmission coefficient between the transverse and longitudinal waves with $\eta = 39.0$ Å is seen in Fig. 11. The transmission coefficients for the cases of $D = 14$ and 33 Å without the SC molecules is higher for the longitudinal mode than for the transverse mode. To investigate further the mechanisms of the difference, we depict in Fig. 12 the time evolution of the displacement of the transmitted wave with $\eta = 39.0$ Å in the polymer sub-system for the cases of $D = 14$ Å with and without the SC molecules ($D$ is slightly larger than 14 Å after addition of the SC molecules). In each panel of Fig. 12, the solid and dashed curves correspond respectively to the left and right end-regions (5 Å width) in the polymer sub-system. The displacements are normalized by $A$ in Eq. (8). Figures 12 (a) and 12 (c) show the results for the case without the SC molecules for the longitudinal and transverse modes, respectively. For the longitudinal mode, the maximum displacement in the left end-region of the polymer sub-system is the same as the one of the α-alumina due to the volume change nature of the mode. However displacement of the right end-region becomes quite small, which means that the longitudinal mode dissipates quickly in the polymer sub-system. For the transverse mode, the maximum displacement in the polymer sub-system is 0.16 as seen in Fig. 12 (c), which is much smaller than in the longitudinal mode. However, displacement of the right end-region is the same order as that of the left end-region with the phase shifted significantly, which is a reflection of relatively slow group velocity of the wave in the polymer sub-system.

Third we analyze the effects of SC molecules on the transmission coefficient. Figures 12 (b) and 12 (d) depict the displacements of the polymer sub-system in the case of $D = 14$ Å with the SC molecules for the wave packet with $\eta = 39.0$ Å in the longitudinal and transverse modes, respectively. For the longitudinal mode, addition of the SC molecules does not change the transmission coefficient substantially (see Fig. 11). We find in Fig. 12 (b) that the displacement in the right end-region is similar to the case without the SC molecules for the longitudinal mode. On the other hand, the transmission coefficient in the transverse mode is increased substantially by addition of the SC molecules (see Fig. 11). The transverse wave has the maximum displacement 2.25 times as large as that in the case without the SC molecules as seen in Fig. 12 (d). In addition, the wave in the right end-region appears to have little phase shift. We therefore conclude that addition of the SC molecules makes the transverse phonons transfer better with faster group velocities in the polymer sub-system. It is in accord with the statement that the bisA molecules in the polymer sub-system are stiffened effectively by addition of the SC molecules. Possible reason of the significant effect of the SC molecules on the transverse wave is that the SC molecules bond

vertically to the surface α-alumina and hence work as resistance to the displacement parallel to the surface in the transverse mode.

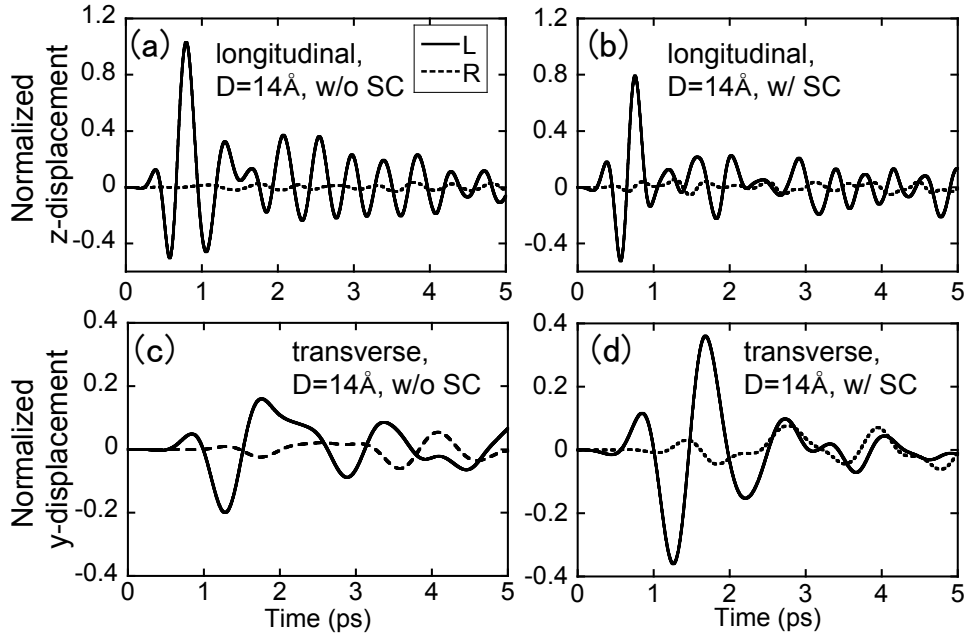


FIG.12

FIG. 12. The time evolutions of $z$ and $y$-displacements at the left (L) and right (R) end-regions of the polymer sub-system in various cases of the wave-packet dynamics simulation: (a) for longitudinal mode in the case of $D = 14$ Å without the SC; (b) for longitudinal mode in the case of $D = 14$ Å with the SC; (c) for transverse mode in the case of $D = 14$ Å without the SC; (d) for transverse mode in the case of $D = 14$ Å with the SC.

## 6. DISCUSSION AND CONCLUDING REMARKS

The overall thermal conductivity of the polymer-ceramic composite at a relatively high packing fraction of the ceramic fillers depends mainly on the effective thermal conductivities of the sandwiched polymer regions. Motivated by that we have performed the NEMD simulation to obtain the effective thermal conductivity of such a system, in which the bisA polymer sub-system with depth $14 - 70$ Å has been inserted between two $\alpha$-alumina slabs. Effects of the SC agent have also been investigated by adding model molecules to the polymer sub-system. For smaller polymer-depth cases, the effective thermal conductivity is determined essentially by the interfacial thermal conductance relating to the temperature-gaps at the interfaces. Through the NEMD simulation, we have found for the interfacial thermal conductance that: (i) it is decreased by decreasing the polymer depth toward the chain length of a single bisA molecule, and (ii) it is

increased by adding the SC molecule to the polymer sub-system.

Through detailed analyses of the polymer configurations, we have shown that the finding (i) has resulted from the decrease in the phonon transmission coefficient relating to effectively weakened interaction between a bisA molecule and two α-alumina slabs. The weakening has resulted because the orientation constraint on the bisA molecule due to attachment of each of the two epoxy groups to each of the two α-alumina slabs, lowers the density of the bisA atoms at the interface. As for the finding (ii), we have found three mutually relating reasons through the atomic vibrational spectra analyses and the phonon wave-packet dynamics simulation. First the phonon population of the bisA molecules at those frequencies corresponding to that of acoustic phonons of α-alumina is enhanced by addition of the SC molecules. The bisA molecules become effectively stiffer through entanglement of the bisA and SC molecules. Second the phonon transmission coefficient from the α-alumina slab to the polymer sub-system is increased significantly for the transverse acoustic mode by addition of the SC molecules bonding to surface Al's of α-alumina. The vertical bonding of the SC molecules to the α-alumina surface works as resistance to the displacement parallel to the surface in the transverse mode. Third the group velocities of transverse acoustic mode are increased by addition of the SC molecules due to their roles of the resistance.

It is interesting to compare the present results with theoretical predictions with respects to the phonon transmission coefficient ($t_{ab}$) and the interfacial thermal conductance ($J/\Delta T$). As for the transmission coefficient, two theoretical models are well known: the acoustic mismatch model (AMM) [14] and the diffuse mismatch model (DMM) [15]. Continuity of both displacement and stress at the interface gives the AMM transmission coefficient for the phonon with frequency in the common frequency range as $t_{ab}^{\mathrm{AMM}} = 4Z_aZ_b\mu_a\mu_b/(Z_a\mu_a + Z_b\mu_b)^2$, where the impedence $Z_i = n_iv_i$ with the number density of atoms $n_i$ and the group velocity $v_i$, and $\mu_i = \cos\theta_i$ with the incident angle $\theta_i$. In the DMM, the phonons scattered at the interface are assumed to lose fully the information of the incident directions. The $t_{ab}^{\mathrm{DMM}} = v_{\mathrm{b}}g_b(f)/[v_ag_a(f) + v_bg_b(f)]$ with the phonon density-of-state $g_i(f)$. Setting $v_b/v_a = 0.18$, $Z_b/Z_a = 0.04$, and $\theta_a = \theta_b = 0$ for the present interface (medium-$a$ is the α-alumina, medium-$b$ is the polymers), we find $t_{ab}^{\mathrm{AMM}} = 0.16$. The $t_{ab}^{\mathrm{DMM}} = 0.03$ using the Debye approximation for phonons. The transmission coefficient for the longitudinal acoustic phonon with $\eta = 39.0$ Å in the case of $D = 33.0$ Å without the SC molecules is about 0.09 (see Fig. 11), which indicates a tendency to approach the $t_{ab}^{\mathrm{AMM}}$ at longer $\eta$. Similar observations for the longitudinal acoustic phonons were reported also for other systems as the grain boundary of Si and the interface of the Lennard-Jones solids with different atomic masses, through the wave-packet dynamics simulations [14, 42]. As expected, the present transmission coefficients at a short wavelength of $\eta = 13.0$ Å (see Fig. 11) compare well with the

$t_{ab}^{\mathrm{DMM}}$.

As for the interfacial thermal conductance, the Landauer formula [14,43] that uses the equilibrium phonon population ($P$) at the local temperature, has commonly been used: $(J/\Delta T)_{\mathrm{Landauer}} = \frac{1}{V_a}\sum^{+}_{\mathrm{mode},\vec{\eta}} v_{a,z}(\mathrm{mode},\vec{\eta}) h f_a(\mathrm{mode},\vec{\eta})[dP_a(T_a,\mathrm{mode},\vec{\eta})/dT_a] t_{ab}(\mathrm{mode},\vec{\eta})$. The Landauer formula gives $3.5\ \mathrm{MW/K\cdot m^2}$ for the AMM and $12.6\ \mathrm{MW/K\cdot m^2}$ for the DMM [14]. Those are much smaller than the present values of $100-250\ \mathrm{MW/K\cdot m^2}$ in Fig. 4 (b). Limitations of the Landauer formula are well known, including the paradox that the formula gives a finite conductance even for the virtual interface with identical sub-systems [13,14,19,44]. The paradox is due to ignorance of non- equilibrium nature of $P$, that is, the $P$ at a given location should be affected by the ones within the range of the phonon mean free-path. The analytical formulas that take into account such non-equilibrium effects in $P$ [14], predict larger values than the Landauer ones: $3.6\ \mathrm{MW/K\cdot m^2}$ for the AMM and $14.0\ \mathrm{MW/K\cdot m^2}$ for the DMM. Those values are still much smaller than the present ones. The significant differences indicate importance of atomic scale inhomogeneity and anisotropicity to predict the interfacial thermal conductance of the present model, as well as inappropriateness of the phonon picture in the polymer sub-system.

There exist a number of issues that need be improved in future researches: (i) We have used one of the simplest model molecules (see Fig. 1) for the bisphenol-A epoxy polymer and surface-coupling agent in the present study. Depending on the application, the bisphenol-A epoxy polymers are controlled to polymerize and cross-link with other molecules. (ii) The bond-formation reactions of surface-coupling molecules with filler material are complex combinations of hydrolysis and condensation reactions. We have adopted the ideal situation of bonding between the O in the SC molecule and Al of α-alumina in the present study. (iii) In the phonon wave-packet dynamics simulation, to trace the time-evolution of kinetic and potential energy, the system is cooled down to nearly zero temperature before adding the initial wave-packet with quite small amplitude. In the situation, the phonons experience little anharmonicity of the inter-atomic potential and the polymer configuration differs much from the one at a finite temperature. As for the issues (i) and (ii), the first-principle MD simulation [45] or hybrid quantum-classical simulation [46,47], in which reacting atoms are treated with the DFT method, can be used for improvement albeit requiring high computation power. Relating to the issue (iii), we can take ensemble of atomic configurations at a finite temperature with the static inverted forces added on all atoms to fix them. The phonon wave-packet dynamics simulation in such systems can be an improvement.

**ACKNOWLEDGEMENTS**

This research is supported by MEXT Strategic Programs for Innovative Research (SPIRE), Computational Materials Science Initiative (CMSI), High Performance Computing Infrastructure (HPCI) of RIST (hp120123, hp13022, hp140096, hp140214, hp150041), and Grant-in-Aid for Scientific Research (Kakenhi: 23310074) of Japan. The computations were performed using Fujitsu FX10 at Information Technology Center of University of Tokyo, Fujitsu FX10 at Institute for Solid State Physics of University of Tokyo, Hitachi SR16000 at Institute of Material Research of Tohoku University, Fujitsu FX1 and FX10 at Information Technology Center of Nagoya University, and Fujitsu PRIMERGY at Research Center for Computational Science (Okazaki).

**REFERENCES**


[1] S. Mallik, N. Ekere, C. Best, and R. Bhatti, Investigation of thermal management materials for automotive electronic control units, Appl. Thermal Eng. 31(2011) 355-362.

[2] X. C. Tong, Advanced Materials for Thermal Management of Electronic Packaging, New York: Springer; 2011.

[3] R. W. Johnson, J. L. Evans, P. Jacobsen, J. R. Thompson, and M. Christopher, The changing automotive environment: high-temperature electronics, IEEE Trans. Electro. Pack. Manuf. 27 (2004) 164-176.

[4] X. Lu and G. Xu, Thermally conductive polymer composites for electronic packaging, J. Appl. Polym. Sci. 65 (1997) 2733-2738.

[5] D. W. Sundstrom and Y. D. Lee, Thermal conductivity of polymers filled with particulate solids, J. Appl. Polym. Sci. 16(1972) 3159-3167.

[6] Z. Shi, M. Radwan, S. Kirihara, Y. Miyamoto, and Z. Jin, Enhanced thermal conductivity of polymer composites filled with three-dimensional brushlike AlN nanowhiskers, Appl. Phys. Lett. 95 (2009) 224104.

[7] Y. Agari, A. Uneda, and S. Nagai, Thermal conductivity of a polymer composite, J. Appl. Polym. Sci. 49 (1993) 1625-1634.

[8] C. P. Wong and R. S. Bollampally, Thermal conductivity, elastic modulus, and coefficient of thermal expansion of polymer composites filled with ceramic particles for electronic packaging, J. Appl. Polym. Sci. 74 (1999) 3396-3403.

[9] Y. S. Xu, D. D. L. Chung, and C. Mroz, Thermally conducting aluminum nitride polymer-matrix composites, Composites Part A: Appl. Sci & Manuf. 32 (2001) 1749 -1757.

[10] H. Hirano, J. Kadota, T. Yamashita, and Y. Agari, Treatment of inorganic filler surface by silane-coupling agent: investigation of treatment condition and analysis of bonding state of reacted agent, Int. J. Chem. Biol. Eng. 6 (2012) 29-33.

[11] P. L. Kapitza, The study of heat transfer in helium II, J. Phys. USSR 4 (1941) 1-31.

[12] E. T. Swartz and R. O. Pohl, Thermal boundary resistance, Rev. Mod. Phys. 61 (1989) 605 -668.

[13] S. Pettersson and G. D. Mahan, Theory of the thermal boundary resistance between dissimilar lattices, Phys. Rev. B 42 (1990) 7386-7390.

[14] S. Merabia and K. Termentzidis, Thermal conductance at the interface between crystals using equilibrium and nonequilibrium molecular dynamics, Phys. Rev. B 86 (2012) 094303; J. Phys.: Conf. Ser. 395 (2012) 012115.

[15] D. G. Cahill, W. K. Ford, K. E. Goodson, G. D. Mahan, A. Majumdar, H. J. Maris, R. Merlin, and S. R. Philpot, Nanoscale thermal transport, J. Appl. Phys. 93 (2003) 793-818.

[16] K. Sasikumar and P. Keblinski, Effect of chain conformation in the phonon transport across a Si-polyethylene single-molecule covalent junction, J. Appl. Phys. 109 (2011) 114307.

[17] M. Hu, S. Shenogin, and P. Keblinski, Molecular dynamics simulation of interfacial thermal conductance between silicon and amorphous polyethylene, Appl. Phys. Lett. 91 (2007) 241910.

[18] T. Luo and J. R. Llyd, Enhancement of thermal energy transport across graphene/graphite and polymer interfaces: A molecular dynamics study, J. Adv. Funct. Mater. 22 (2012) 2495-2502.

[19] E. S. Landry and A. J. H. McGaughey, Thermal boundary resistance predictions from molecular dynamics simulations and theoretical calculations, Phys. Rev. B 80 (2009) 165304.

[20] K. Tanaka, S. Ogata, R. Kobayashi, T. Tamura, M. kitsunezuka, and A. Shinma, Enhanced heat transfer through filler-polymer interface by surface-coupling agent in heat-dissipation material: A non-equilibrium molecular dynamics study, J. Appl. Phys. 114 (2013) 193512.

[21] S. Maruyama, A molecular dynamics simulation of heat conduction of a finite length single-walled carbon nanotube, Microscale Thermophys. Eng. 7 (2003) 41-50.

[22] J. Shiomi, and S. Maruyama, Non-Fourier heat conduction in a single-walled carbon nanotube: Classical molecular dynamics simulations, Phys. Rev. B 73 (2006) 205420.

[23] P. K. Schelling S. R. Phillpot, and P. Keblinski, Phonon wave-packet dynamics at semiconductor interfaces by molecular-dynamics simulation, Appl. Phys. Lett. 80 (2002) 2484-2486.

[24] P. K. Schelling, S. R. Phillpot, and P. Keblinski, Kapitza conductance and phonon scattering at grain boundaries by simulation, J. Appl. Phys. 95 (2004) 6082-6091.

[25] Z. T. Tian, B. White, and Y. sun, Phonon wave-packet interference and phonon tunneling based energy transport across nanostructured thin films, Appl. Phys. Lett. 96 (2010) 26113.

[26] N. A. Roberts and D. G. Walker, Phonon wave-packet simulations of Ar/Kr interfaces for thermal rectification, J. Appl. Phys. 108 (2010) 123515.

[27] S. R. White, P. T. Mather, and M. J. Smith, Characterization of the cure-state of DGEBA-DDS epoxy using ultrasonic, dynamic mechanical, and thermal probes, Polym. Eng. Sci. 42 (2002) 51-67.

[28] J. F. Fu, L. Y. Shi, Q. D. Zhong, Y. Chen, and L-Y, Chen, Thermally conductive and electrically insulative nanocomposites based on hyperbranched epoxy and nano-$Al_2O_3$ particles modified epoxy resin, Polym. Adv. Tecnol. 22 (2010) 1032.

[29] K. C. Hass, W. F. Schneider, A. Curioni, and W. Andreoni, The chemistry of water on alumina surfaces: Reaction dynamics from first principles, Science 282 (1998) 265-268.

[30] I. Frank, D. Marx, and M. Parrinello, Structure and electronic properties of quinizarin

chemisorbed on alumina, J. Chem.Phys. 104 (1996) 8143 -8150.

[31] I. Manassidis, A. DeVita, and M. J. Gllian, Structure of the (0001) surface of $\alpha$-$Al_2O_3$ from first principles calculations, Surf. Sci. Lett. 285 (1993) 517-521.

[32] J. P. Pascault and R. J. J. Williams, Epoxy polymer, New Jersey: Wiley; 2010.

[33] C. Li, G. A. Medvedev, E-W. Lee, J. Kim, J. M. Caruthers, and A. Strachan, Molecular dynamics simulations and experimental studies of the thermomechanical response of an epoxy thermoset polymer, Polymer 53 (2012) 4222-4230.

[34] B. Arab and A. Shokuhfar, Molecular dynamics simulation of cross-linked epoxy polymers: the effect of force field on the estimation of properties, J. Nano-Electronic Phys. 5 (2013) 01013.

[35] M. Matsui, Molecular dynamics study of the structures and bulk moduli of crystals in the system CaO-MgO-$Al_2O_3$-$SiO_2$, Phys. Chem. Minerals 23 (1996) 345-353.

[36] S. L. Mayo, B. D. Olafson, and W. A. Goddard III, DREIDING: A generic force field for molecular simulations, J. Phys. Chem. 94 (1990) 8897-8909.

[37] J. Gasteiger and M. Marsili, Iterative partial equalization of orbital electronegativity: a rapid access to atomic charges, Tetrahedron, 36 (1980) 3219-3228.

[38] I. C. Yeh and M. L. Berkowitz, Ewald summation for systems with slab geometry, J. Chem. Phys. 117 (1999) 3155-3162.

[39] M. P. Allen and D. J. Tildesley, Computer Simulation of Liquids, Oxford: Clarendon; 1987.

[40] B. Li, L. Wang, and G. Casati, Thermal Diode: Rectification of Heat Flux. Phys. Rev. Lett. 93 (2004) 184301.

[41] M. Hu, P. Keblinski, and B. Li, Thermal rectification at silicon-amorphous polyethylene interface, Appl. Phys. Lett. 92 (2008) 211908.

[42] S.Aubry, C. J. Kimmer, A. Skye, and P. K. Schelling, Comparison of theoretical and simulation-based predictions of grain-boundary Kapitza conductance in silicon, Phys. Rev. B 78 (2008) 064112.

[43] R. Landauer, Electrical resistance of disordered one-dimensional lattices, Philos. Mag, 21 (1970) 863-867.

[44] S. Simons, On the thermal contact resistance between insulators, J. Phys. C 7 (1974) 4048-4052.

[45] S. Ogata, N. Ohba, and T. Kouno, Multi-thousand-atom DFT simulation of Li-ion transfer through the boundary between the solid–electrolyte interface and liquid electrolyte in a Li-ion battery, J. Phys. Chem. C 117 (2013) 17960.

[46] S. Ogata, Buffered-cluster method for hybridization of density-functional theory and classical molecular dynamics: Application to stress-dependent reaction of $H_2O$ on nanostructured Si, Phys.

Rev. B 72 (2005) 045348.

[47] S. Ogata, Y. Abe, N. Ohba, R. Kobayashi, Stress-induced nano-oxidation of silicon by diamond-tip in moisture environment: A hybrid quantum-classical simulation study, J. Appl. Phys. 108 (2010) 064313.